

The hadronic light by light contribution to the $(g - 2)_\mu$ with holographic models of QCD

Luigi Cappiello^{1,2}, Oscar Catà³ and Giancarlo D'Ambrosio²

¹*Dipartimento di Scienze Fisiche, Università di Napoli "Federico II", Via Cintia, 80126 Napoli, Italia*

²*INFN-Sezione di Napoli, Via Cintia, 80126 Napoli, Italia and*

³*Departament de Física Teòrica and IFIC, Universitat de València-CSIC, Apt. Correus 22085, E-46071 València, Spain*

We present a new determination of the hadronic light by light scattering contribution to the muon anomalous magnetic moment, focussing on the (dominant) pion exchange diagram. We use as input the existing experimental low energy data on the anomalous electromagnetic pion form factor $F_{\pi^0\gamma^*\gamma^*}$, QCD short distance constraints and, additionally, predictions coming from holographic models of QCD. Our main goal is to quantify the theoretical uncertainty in $(g - 2)_\mu$ coming from experimental input, QCD short distances and model dependences. In our analysis we will use the parameterization originally introduced by D'Ambrosio, Isidori and Portolés (DIP) to study kaon decays. This will allow us to estimate the impact of the pion being off-shell, which is the relevant kinematical regime for $(g - 2)_\mu$. Our final result is $a_\mu^{\pi^0} = 6.54(25) \cdot 10^{-10}$, where the error is driven by the slope of $F_{\pi^0\gamma^*\gamma^*}$, soon to be measured with precision at KLOE-2. Our numerical analysis also indicates that large values of the magnetic susceptibility χ_0 are disfavored. However, in the absence of stronger bounds on χ_0 , an additional (10 – 15%) systematic uncertainty on the previous value for $a_\mu^{\pi^0}$ cannot be excluded. Additionally, it is shown that holographic predictions for $F_{\pi^0\gamma^*\gamma^*}$ at low energies satisfy to a very good approximation the leading DIP *high energy* constraint. Thus, this relation between long and short distances can be used as a phenomenological prediction for quartic low energy parameters, currently out of experimental reach.

PACS numbers: 14.60.Ef, 13.40.Em, 11.25.Tq

I. INTRODUCTION

The anomalous magnetic moment of the muon is presently one of the most stringent tests of the standard model and, due to the current experimental precision, a very useful tool in the search for new physics. As of today, a discrepancy of roughly three standard deviations persists between the standard model estimate and the experimental value at Brookhaven [1]. Whether this is to be ascribed to evidence for new physics depends crucially on the reliability of the standard model computation.

With the electroweak corrections under good control, the main source of uncertainty on the theoretical side comes from the hadronic contributions, namely the vacuum and the light-by-light contributions. While information on the hadronic vacuum polarization can be extracted from experimental data on the hadronic e^+e^- cross section, the hadronic light-by-light contribution can only be estimated through nonperturbative theoretical methods, *i.e.* lattice simulations and hadronic models. Due to the complexity of the calculation, a lattice result is unfortunately still not available and one has to resort to the latter.

In the past there have been plenty of determinations based on particular models like the ENJL [2], HLS [3] and more recently on different models inspired by the $1/N_c$ expansion under the assumption

of lowest meson dominance (LMD) [4–6]. Different as they are in nature, all the abovementioned models eventually determine their free parameters imposing constraints, either theoretical or experimental. Therefore, the source of uncertainty generally depends on: (i) the experimental input used; (ii) the different theoretical constraints imposed; and (iii) an intrinsic model dependence, which is very difficult to estimate. While it is certainly reassuring that, ever since the seminal paper of Ref. [7] settled an important sign issue, the results for the different models lie in the same ballpark and no big disagreement is present, there are certain unresolved issues that might affect the theoretical error estimate (see for instance the recent discussion in [8]). With the proposals at Fermilab [9], J-PARC [10] and potentially at Frascati [11], the increase in experimental precision will aim at reaching $1.5 \cdot 10^{-10}$ accuracy. Therefore, a reliable estimate of the theoretical error in the hadronic light-by-light contribution becomes of the outmost importance (see, for instance, the recent assessments of the error budget given in Refs. [12, 13]).

In this paper we propose to use the holographic principle [14] to address such issues. Holographic models of QCD, while also based on the $1/N_c$ expansion, offer several advantages over four dimensional LMD models. First and foremost, AdS/QCD models are implemented at the Lagrangian level, and therefore Ward identities between correlators are au-

tomatically fulfilled. Second, due to the AdS metric, short distance matching to asymptotically free QCD is easily achieved. Third, hadronic resonances in AdS/QCD models arise as the Kaluza-Klein states in the process of compactification from five to four dimensions. Therefore, as opposed to LMD models, the full tower of states is automatically implemented and its separate contributions can be analysed. Thus, one can check whether LMD is justified or not. Finally, even though an infinite number of resonances is present, the number of free parameters is very small. Thus, unlike phenomenological hadronic models, very few input is needed in order to be predictive.

Holography therefore has the potential to become a consistent hadronic model for all the hadronic light-by-light contributions to $(g-2)_\mu$, at least at leading order in the $1/N_c$ expansion, *i.e.*, in the limit of single resonance exchange.

In this paper we will concentrate on the neutral pion exchange contribution. We will start by studying the electromagnetic pion form factor $F_{\pi^0\gamma^*\gamma^*}$ in a set of holographic models, which mostly differ in the way they incorporate chiral symmetry breaking. This will allow us to test the models against existing experimental data. In particular, we will compare our values for the slope a_π with the results from CELLO [15]. Agreement with experiment will be used as a filtering criteria for the different models. For those models, predictions for the curvature in both $\pi^0 \rightarrow \gamma^*\gamma$ and $\pi^0 \rightarrow \gamma^*\gamma^*$ will be provided. These predictions can be tested in future experiments, especially in the potential upgrade of the DAΦNE accelerator in Frascati [11].

It should be noted at this point that the pion form factor as built from $F_{\pi^0\gamma^*\gamma^*}$ is not what should be used to evaluate the pion exchange contribution to the hadronic light-by-light scattering. The reason, as recently emphasized in [6, 16, 17], is that the pion in the $(g-2)_\mu$ is off-shell.

The strategy we will follow to bypass this difficulty is to work with an interpolator, first considered in the context of $K_L \rightarrow \mu^+\mu^-$ decays [18], in such a way that it captures the wanted ingredients from the holographic form factor while correcting for the pion off-shellness. In particular, we will be able to incorporate the short distance constraint discussed in [6]. By varying the combination of constraints to be imposed, such an interpolator will allow us to test the stability of our results and estimate the size of the uncertainties associated with experimental and theoretical input, including the one associated with model dependences. Even though in this paper we concentrate our efforts on the anomalous form factor and $(g-2)_\mu$, some of our results are potentially useful for low energy analyses of leptonic and semileptonic kaon decays.

This paper is organized as follows: in Section II we will briefly review the holographic principle and its most common realizations to study QCD. These models will then be used in Section III to study the $\pi^0\gamma\gamma$ form factor, with special emphasis on its low energy predictions. In Section IV we will give an estimate of the pion exchange contribution to the hadronic light-by-light piece of $(g-2)_\mu$. Finally, conclusions will be given in Section V.

II. HOLOGRAPHIC MODELS OF QCD

The AdS/CFT conjecture [14] offers one of the most promising ways to study gauge theories in strongly coupled regimes through their weakly coupled supergravity duals compactified in AdS_5 . In the recent years attempts have been directed towards using the gauge/string duality to QCD, *i.e.*, an holographic equivalence is conjectured between four-dimensional strongly coupled QCD at large N_c and a five-dimensional weakly interacting gauge theory coupled to gravity on a five-dimensional space not necessarily (but asymptotically) AdS_5 . The fact that QCD is conformally invariant in the deep Euclidean makes the gauge/string duality a good starting point towards a theory of hadrons. However, QCD is not conformal in the strongly coupled regime and crucial ingredients like confinement or chiral symmetry breaking have to be incorporated. Confinement can be easily modeled by making the bulk space compact, for instance by placing an infrared brane some distance z_0 away from the ultraviolet brane. The QCD resonances are then the Kaluza-Klein modes arising from the compactification. Chiral symmetry breaking is more involved but AdS/CFT seems to have the potential to describe both explicit and spontaneous symmetry breaking [19]. The pion field can also be incorporated, and the agreement of the whole picture with QCD, especially with vector mesons, is quite remarkable [20–23].

In order to bridge the gap between the original AdS/CFT conjecture and AdS/QCD two main approaches have been followed, so-called top-down and bottom-up. In the top-down approach, one looks for a suitable setting of D-branes in string theory, with gauge theory on their world-volume, which at low energy would produce an effective background geometry for the dual five-dimensional gravitational theory. An example is the Sakai-Sugimoto model [22] to be considered later.

The bottom-up approach is more phenomenologically oriented and one starts directly from warped five-dimensional models, with an AdS_5 metric in the ultraviolet regime but with drastic deviations in the infrared, where non-perturbative effects of

QCD force a description in terms of new low energy degrees of freedom. In this paper we will consider Hard-Wall (HW) and Soft-Wall (SW) models. Both in the Hard-Wall (HW) models of [20] and [24], the AdS_5 space is cut off at a finite size, producing an infinite number of Kaluza-Klein resonances, to be identified with the hadronic spectrum. The two models differ in the implementation of χSB , though. In [20], χSB is induced by a 5D scalar field, holographically dual of the $\bar{q}q$ operator of QCD, whose non vanishing vacuum expectation value is responsible for χSB . In contrast, in [24], χSB is achieved by imposing appropriate infrared boundary conditions. The Soft-Wall (SW) model proposed in [25] is a five-dimensional holographic model in which the AdS_5 space is non-compact. Confinement and an infinite number of bound states follow from the presence of a non-trivial dilaton background. The main feature of the SW model is its ability to produce an hadronic spectrum with Regge behavior, which leads to better agreement with the resonance spectrum in QCD.

In any of the models above, one boldly conjectures the applicability of the holographic recipe to compute correlation functions of the dual 4-dimensional

theory [26, 27]. For every quantum operator $\mathcal{O}(x)$ in QCD, there exists a corresponding bulk field $\phi(x, z)$, whose value on the ultraviolet brane, $\phi(x, 0) \equiv \phi_0(x)$, is identified with the four-dimensional source of $\mathcal{O}(x)$. Hence, the generating functional of the four-dimensional theory can be computed from the five-dimensional action evaluated *on-shell* (neglecting stringy corrections), *i.e.*,

$$\exp(iS_5[\phi_0(x)]) = \langle \exp \left[i \int d^4x \phi_0(x) \mathcal{O}(x) \right] \rangle_{\text{QCD}_4} . \quad (1)$$

Integrating by parts the quadratic part of the five-dimensional action on-shell effectively reduces to a boundary four-dimensional term quadratic in $\phi_0(x)$. By varying the action with respect to $\phi_0(x)$ one can generate the different connected n -point Green's functions of QCD.

The simplest five-dimensional action can be generically written in the form

$$S_5 = S_{\text{YM}} + S_X + S_{\text{CS}} , \quad (2)$$

where

$$\begin{aligned} S_{\text{YM}} &= -\text{tr} \int d^4x \int_0^{z_0} dz e^{-\Phi(z)} \frac{1}{8g_5^2} w(z) \left[\mathcal{F}_{(L)}^{MN} \mathcal{F}_{(L)MN} + \mathcal{F}_{(R)}^{MN} \mathcal{F}_{(R)MN} \right] , \\ S_X &= \text{tr} \int d^4x \int_0^{z_0} dz e^{-\Phi(z)} w(z)^3 \left[D^M X D_M X^\dagger + V(X^\dagger X) \right] , \end{aligned} \quad (3)$$

with $\mathcal{F}_{\mu\nu} = \partial_\mu \mathcal{B}_\nu - \partial_\nu \mathcal{B}_\mu - i[\mathcal{B}_\mu, \mathcal{B}_\nu]$ and $\mathcal{B}_{L,R} = V \mp A$ where $V(A) \in U(2)_{V(A)}$ are vector (axial-vector) five-dimensional fields. If these are coupled to Dirac currents, then the holographic prescription predicts that they are massless and hence gauge-invariant. It is common to work in the axial gauge $V_5 = A_5 = 0$. The surviving five-dimensional gauge fields $V_\mu(x, z)$ and $A_\mu(x, z)$ holographically correspond to four-dimensional vector and axial-vector QCD currents, $\bar{q}\gamma_\mu q$ and $\bar{q}_R\gamma_\mu\gamma_5 q_R$, respectively.

$\Phi(z)$ is a dilaton field and $X(x, z)$ a scalar field transforming under the chiral group as $g_L X g_R^\dagger$. Then, accordingly, $D_M X = \partial_M X - iL_M X + iX R_M$. As we shall see below, the presence of the scalar field X and the form of its potential depend on the model considered. For instance, in models where χSB is induced by chirally-asymmetric boundary conditions on the gauge fields, $X(x, z)$ is not essential.

The extra-dimension is taken to extend over the interval $(0, z_0)$, where the upper limit can be infinite

for some models. The metric of the five-dimensional space can be written generically in terms of a warp factor $w(z)$ as

$$g_{MN} dx^M dx^N = w(z)^2 (\eta_{\mu\nu} dx^\mu dx^\nu - dz^2) , \quad (4)$$

where $\eta_{\mu\nu} = \text{Diag}(1, -1, -1, -1)$, $\mu, \nu = (0, 1, 2, 3)$ and $M, N = (0, 1, 2, 3, z)$. In AdS_5 space the warping factor takes the form $w(z) = 1/z$.

As pointed out in [28], anomalous processes in four dimensions can be reproduced from the five-dimensional Chern-Simons term

$$S_{\text{CS}}[\mathcal{B}] = \frac{N_c}{24\pi^2} \int \text{tr} \left(\mathcal{B} \mathcal{F}^2 - \frac{i}{2} \mathcal{B}^3 \mathcal{F} - \frac{1}{10} \mathcal{B}^5 \right) . \quad (5)$$

In order to account for chirality, one should work with

$$S_{\text{CS}}^{\text{AdS}}[\mathcal{B}_L, \mathcal{B}_R] = S_{\text{CS}}[\mathcal{B}_L] - S_{\text{CS}}[\mathcal{B}_R] . \quad (6)$$

In the following we will briefly review the general features of the holographic models we will consider

for our analysis of the electromagnetic pion form factor, mainly to fix our notation. Further details can be found in the original literature.

A. Hard-Wall models

The distinguishing features of Hard-Wall (HW) models are a compact fifth dimension, $0 \leq z \leq z_0$ and a constant dilaton field $\Phi(z)$. We will concentrate on two such models, which we name HW1 [20, 21] and HW2 [24]. The presence of the upper bound $z = z_0$ defines an infrared brane, producing an explicit breaking of the scale invariance of the dual four-dimensional theories at energies $\approx 1/z_0 \approx 1$ GeV. Moreover, in the presence of this cut-off, Wilson loops follows an area-law behavior in the infrared regime, thereby simulating the onset of a confining phase.

In compliance with χ SB in the four-dimensional theory, axial gauge invariance is broken in the five-dimensional background, the longitudinal component of the axial-vector field becoming physical and related to the pion field.

HW1 and HW2 differ in the mechanism leading to the χ SB. In the HW1 model, the breaking is due to the scalar field $X(x, z)$, whose coupling to the axial-vector gauge field produces an effective mass term, breaking the gauge invariance in the axial sector. In the HW2 model, instead, no such field is present in the five-dimensional Lagrangian (2) and χ SB is achieved through different infrared boundary conditions for vector and axial-vector fields.

1. χ SB from a scalar bulk field: HW1

One considers the action (3) without dilaton field and with the complex scalar field $X(x, z) = v(z)U(x, z)/2$, where U contains the pion field and $v(z)$ is the scalar component that breaks chiral symmetry in the bulk. The scalar potential is reduced to the mass term, given by:

$$V(X^\dagger X) = \frac{3}{z^5} X^\dagger X . \quad (7)$$

The previous expression guarantees that X can be coupled to $\bar{q}q$. Solving the five-dimensional equations of motion at zero four-dimensional momentum one finds $v(z) = (m_q z + \sigma z^3)$, where the parameters m_q and σ are holographically identified as the quark mass and the $\bar{q}q$ condensate, *i.e.* the sources of explicit and spontaneous χ SB, respectively.

A non-vanishing $v(z)$ induces a z -dependent mass term for the axial-vector field in Eq. (3), thereby breaking the degeneracy between vector and axial

vector resonances. The scalar field X also produces a non trivial coupling between the longitudinal component of the axial-vector field and the pion field. Defining $A_{\mu\parallel}^a(q, z) = -iq_\mu \varphi(q, z)$ and $U(x, z) = \exp[2it^a \pi^a(x, z)]$ (for $SU(2)$, $t^a = \sigma^a/2$, with σ^a being the Pauli matrices) one gets the system of coupled equations [20]:

$$\partial_z \left(\frac{1}{z} \partial_z \varphi^a \right) + \frac{g_5^2 v(z)^2}{z^3} (\pi^a - \varphi^a) = 0 , \quad (8)$$

$$-q^2 \partial_z \varphi^a + \frac{g_5^2 v(z)^2}{z^2} \partial_z \pi^a = 0 . \quad (9)$$

As a result, the HW1 model satisfies the Gell-Mann–Oakes–Renner (GMOR) relation [29]:

$$m_\pi^2 f_\pi^2 = (m_u + m_d) \langle \bar{q}q \rangle = 2m_q \sigma . \quad (10)$$

The pion wave function $\varphi(z) = 1 - \Psi(z)$ can be obtained from the coupled equations (8) and (9) which describe the dynamics in the axial sector. In the chiral limit, $m_q = 0$, one obtains

$$\Psi(z) = \Gamma[2/3] \left(\frac{\xi}{2} \right)^{\frac{1}{3}} \left[1 - \frac{I_{2/3}(\xi z_0^3)}{I_{-2/3}(\xi z_0^3)} \right] z I_{-1/3}(\xi z^3) , \quad (11)$$

where $\xi \equiv g_5 \sigma / 3$, σ being the quark condensate. The pion wave function is different from zero on the infrared brane,

$$\Psi(z_0) = \frac{\sqrt{3}\Gamma[2/3]}{\pi I_{-2/3}(\xi)} \left(\frac{1}{2\xi^2} \right)^{1/3} , \quad (12)$$

a fact that will be important in the evaluation of the anomalous amplitude.

By solving the equation of motion for the vector field ($Q^2 = -p^2$ being the 4-dimensional Euclidean momentum):

$$\partial_z \left(\frac{1}{z} \partial_z \mathcal{J} \right) - \frac{Q^2}{z} \mathcal{J} = 0 , \quad (13)$$

subject to the (Dirichlet) ultraviolet boundary condition $\mathcal{J}(Q, 0) = 1$ and the (Neumann) infrared one, $\partial_y \mathcal{J}(Q, z_0) = 0$, one finds the so-called vector bulk-to-boundary propagator $\mathcal{J}(Q, z)$, which can be written in terms of Bessel functions:

$$\mathcal{J}(Q, z) = Qz \left[K_1(Qz) + I_1(Qz) \frac{K_0(Qz_0)}{I_0(Qz_0)} \right] . \quad (14)$$

Vector resonances are associated with solutions $\psi_n(z)$ of the equation of motion for the vector field at discrete $p^2 = m_n^2$, with vanishing boundary conditions: $\psi_n(0) = 0$, and $\partial_z \psi_n(z_0) = 0$.

2. χ SB through boundary conditions: HW2

The action of the HW2 model [24] is entirely given by the gauge field part of eq.(3). The role of the scalar field X as the source of chiral symmetry breaking is played by asymmetric boundary conditions between vector and axial fields. In this model, vectors are required to obey infrared Neumann boundary conditions while axial fields satisfy Dirichlet boundary conditions. This leads to a splitting in the mass spectra that qualitatively reproduces what is observed in nature.

The pion field is built from Wilson lines extending between the 5D boundaries:

$$U(x) = \xi_R(x) \xi_L^{-1}(x) , \quad (15)$$

where

$$\xi_{L,R}(x) = P \exp \left\{ -i \int_0^{z_0} dz' \mathcal{B}_z^{L,R}(x, z') \right\} . \quad (16)$$

The fact that the pion is a non-local object leads to difficulties to implement the GMOR relation. For our purposes, this won't be of relevance, since we shall consider the HW2 model only in the chiral limit of massless pions.

Chiral symmetry breaking is implemented by splitting the fields like

$$\begin{aligned} \hat{V}_\mu(x, z) &\equiv V_\mu(x, z) + \hat{V}_\mu(x, 0) , \\ \hat{A}_\mu(x, z) &\equiv A_\mu(x, z) + \alpha(z) \hat{A}_\mu(x, 0) , \end{aligned} \quad (17)$$

where the last terms are the sources and $\alpha(z)$, which plays the role of the pion wave function, is determined by demanding no mixing between the pion and the axial resonances:

$$\alpha(z) = 1 - \frac{z^2}{z_0^2} . \quad (18)$$

For comparison, we will also consider the flat case, *i.e.* $w(z) = 1$. In that case the bulk-to-boundary propagator takes the form

$$\mathcal{J}(Q, z) = \cosh(Qz) + \tanh(Qz_0) \sinh(Qz) , \quad (19)$$

and the pion wave function is given by

$$\alpha(z) = 1 - \frac{z}{z_0} . \quad (20)$$

3. The Sakai-Sugimoto as an HW2 model

The original action of [22] is

$$S = S_{\text{YM}} + S_{\text{CS}} , \quad (21)$$

with

$$S_{\text{YM}} = -\kappa \int d^4x \int_{-\infty}^{\infty} dz \, \text{tr} \left[\frac{1}{2} h(z) \mathcal{F}_{\mu\nu}^2 - k(z) \mathcal{F}_{\mu z}^2 \right] , \quad (22)$$

where the functions $h(z)$ and $k(z)$ are given by

$$h(z) = (1 + z^2)^{-1/3} ; \quad k(z) = 1 + z^2 , \quad (23)$$

and S_{CS} is given in Eq. (6).

The constant κ is related to the 't Hooft coupling λ and the number of colors N_c as

$$\kappa = \frac{\lambda N_c}{216\pi^3} . \quad (24)$$

The model also has a mass scale M_{KK} , which in (22) it was absorbed in the dimensionless parameter z . For our numerical analysis, the two parameters will be chosen as [22]

$$M_{KK} = 949 \text{ MeV} , \quad \kappa = 0.00745 , \quad (25)$$

in order to fit the experimental values of the ρ meson mass, $m_\rho \simeq 776 \text{ MeV}$, and the pion decay constant, $f_\pi \simeq 92.4 \text{ MeV}$.

The action (21) was obtained in [22] as the effective action of N_f probe D8-branes placed in the background of N_c D4-brane, studied in [30], and stands for an effective theory of mesons in four dimensional (large N_c) QCD with N_f massless quarks. In the following we will reformulate the Sakai-Sugimoto model and show that it can be cast in the form of a HW2 model. This reformulation will prove useful for computational purposes in the following Section.

As a first step, let us define $y = \tan^{-1} z$, with values in the finite interval $-\pi/2 \leq y \leq \pi/2$, whose end points $y = \pm\pi/2$ correspond to the ultraviolet branes while the point $y = 0$ corresponds to the infrared brane. In the $A_z = 0$ gauge, (22) becomes

$$S_{\text{YM}} = -\kappa \int d^4x \int_{-\pi/2}^{\pi/2} dy \, \text{tr} \left[\frac{1}{2} \tilde{h}(y) \mathcal{F}_{\mu\nu}^2 - \mathcal{F}_{\mu y}^2 \right] , \quad (26)$$

where $\tilde{h}(y)$ is an *even* function of y . This allows us to decompose the gauge field \mathcal{A}_μ in parity-even and parity-odd parts as $\mathcal{A}_\mu = V_\mu + A_\mu$, with $V_\mu(x, -y) = V_\mu(x, y)$ and $A_\mu(x, -y) = -A_\mu(x, y)$, and restrict the theory to half the interval, *i.e.* $0 \leq y \leq \pi/2$. Parity transformations in the fifth dimension correspond to the exchange of left and right-handed chiralities and can be used to distinguish between vectors and axial vector fields (vectors and axial having even and odd y -profiles, respectively). As a consequence they satisfy different boundary conditions on the infrared brane (at $y = 0$), *i.e.* Neumann for vectors, $\partial_y V_\mu|_{y=0} = 0$, and Dirichlet $A_\mu|_{y=0} = 0$ for axial vectors.

Next, let us define the dimensionless variable $z \equiv \pi/2 - y$, with $0 \leq z \leq \pi/2$ (not to be confused with the original variable in (22)). $z = 0$ corresponds to the ultraviolet brane and $z = \pm\pi/2$ to the infrared brane, and the action takes the following form:

$$S_{\text{YM}} = -\kappa \int d^4x \int_0^{\pi/2} dz \text{tr} \left\{ (\sin z)^{-4/3} \times [(V_{\mu\nu} - i[A_\mu, A_\nu])^2 + (D_\mu A_\nu - D_\nu A_\mu)^2] - 2(\partial_z V_\mu)^2 - 2(\partial_z A_\mu)^2 \right\}, \quad (27)$$

where $V_{\mu\nu} = \partial_\mu V_\nu - \partial_\nu V_\mu - i[V_\mu, V_\nu]$ and $D_\mu A_\nu = \partial_\mu A_\nu - i[V_\mu, A_\nu]$.

In the new variable $z \in [0, \pi/2]$ the SS model takes the form of HW2 model with different boundary conditions for vector and axial vector fields on the infrared boundary $z = \pi/2$, and an effective metric which is not AdS_5 :

$$g_{MN} dx^M dx^N = (\sin z)^{-\frac{4}{3}} \eta_{\mu\nu} dx^\mu dx^\nu - (\sin z)^{-\frac{8}{3}} dz^2. \quad (28)$$

The chiral field containing the pion is also built from Wilson lines extending between boundaries. One can easily show that in the SS model the function $\alpha(z)$ discussed in the previous subsection takes the simple form

$$\alpha(z) = 1 - \frac{2z}{\pi}. \quad (29)$$

Vector (and axial) fields can be obtained by solving the bulk-to-boundary differential equation

$$\left(\frac{d^2}{dz^2} - \frac{Q^2}{(\sin z)^{4/3}} \right) \mathcal{J} = 0, \quad (30)$$

subject to the boundary conditions $\mathcal{J}_{V,A}(Q, 0) = 1$, and $\partial_z \mathcal{J}_V(Q, \pi/2) = 0$, $\mathcal{J}_A(Q, \pi/2) = 0$, for which there is no analytic expression. In Fig. 1 we show the first three normalized eigenfunctions for vector and axial vector field in the new extra-dimensional variable z . As usual, the Fourier transform of the five-dimensional gauge field has been written as $\mathcal{A}_\mu(q, z) = \tilde{\mathcal{A}}_\mu(q) \psi(z)$, with $\psi(z)$ satisfying the equation

$$\psi(z)'' + \frac{q^2}{(\sin z)^{4/3}} \psi(z) = 0. \quad (31)$$

Dynamical resonances $\psi_n(z)$ then correspond to normalized solutions of (31) with $q^2 = m_n^2$, where the normalization condition is given by

$$4\kappa \int_0^{\pi/2} (\sin z)^{-4/3} \psi_m(z) \psi_n(z) dz = \delta_{mn}, \quad (32)$$

to ensure the canonical four-dimensional kinetic term for $\mathcal{A}_\mu(x)$; the discrete spectrum of eigenvalues $q_n \equiv m_n$, with the corresponding eigenfunctions, can then be obtained numerically.

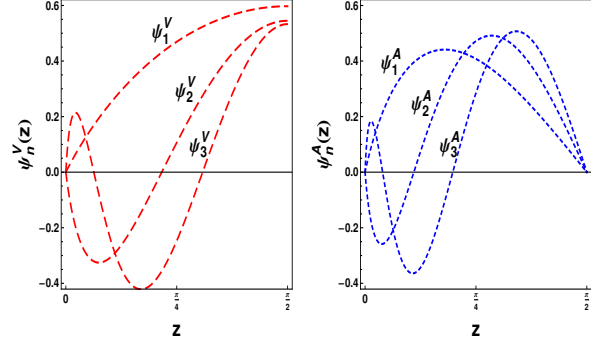


FIG. 1: The first three vector and axial vector meson resonances of the SS model, using the new variable $z \in [0, \pi/2]$.

B. Soft-Wall models

SW models were originally motivated as holographic models with vector resonances displaying Regge trajectories. The action of SW models is given by (2), where the metric is AdS_5 , and $e^{-\Phi(z)}$ represents a non-trivial background dilaton field given by [25]

$$\Phi(z) = \kappa^2 z^2, \quad (33)$$

leading to a spectrum given by

$$m_n^2 = 4\kappa^2(n+1). \quad (34)$$

The dimensionful constant κ can be fixed by fitting the mass of the first vector resonance to that of the ρ meson, *i.e.* $\kappa = m_\rho/2$. Therefore, the equations of motion for the different fields can be obtained from those of the HW1 model by replacing the AdS_5 warp factor with $e^{-\Phi(z)}/z$. Contrary to the HW models, in the SW model the extra-dimension is no longer restricted to a finite interval, *i.e.* $z_0 = \infty$ and the infrared boundary conditions are replaced by normalization conditions on wave functions and bulk-to-boundary propagators.

For the vector fields one has to solve the following equation:

$$\partial_z \left(\frac{e^{-\kappa^2 z^2}}{z} \partial_z \mathcal{J} \right) - Q^2 \frac{e^{-\kappa^2 z^2}}{z} \mathcal{J} = 0, \quad (35)$$

whose solution can be cast in the integral representation [31]

$$\mathcal{J}(Q, z) = \kappa^2 z^2 \int_0^1 \frac{x^a}{(1-x)^2} \exp \left[-\frac{x}{1-x} \kappa^2 z^2 \right] dx, \quad (36)$$

where $a = Q^2/4\kappa^2$.

One of the main drawbacks of the original SW is that chiral symmetry breaking is not implemented in a satisfactory way. Due to the absence of an infrared brane, the parameters for explicit and spontaneous symmetry breaking are not independent, as they should. This not only invalidates general relations like the GMOR, but makes the whole pion dynamics unclear. Recent proposals have tried to circumvent this problem, so far only at an heuristic level. In this paper we will adopt the prescription given in [32], where the pion wave function is assumed to be Gaussian,

$$\alpha(z) = e^{-\kappa^2 z^2}. \quad (37)$$

A comparison of the pion wave function profiles for the different models is shown in Fig. 2.

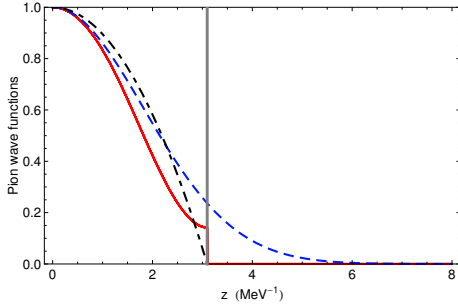


FIG. 2: Comparison of the pion wave functions of the HW1 model (red solid line), the HW2 model (dot-dashed line) and the Gaussian ansatz of Eq. (37) (blue dashed line). The vertical line corresponds to the infrared brane at $z = z_0$.

III. $\pi^0 \gamma^* \gamma^*$ FORM FACTOR

In this section we will apply the methods described previously for the anomalous pion form factor. We will define the $\pi^0 \gamma^* \gamma^*$ form factor as

$$\int d^4x e^{iq_1 \cdot x} \langle 0 | T \{ J_{\text{EM}}^\mu(x) J_{\text{EM}}^\nu(0) \} | \pi^0(p) \rangle \quad (38)$$

$$= \epsilon^{\mu\nu\alpha\beta} q_{1\alpha} q_{2\beta} F_{\gamma^* \gamma^* \pi^0}(Q_1^2, Q_2^2),$$

where $p = q_1 + q_2$ is the pion momentum, q_1, q_2 are the momenta of photons, and $q_{1,2}^2 = -Q_{1,2}^2$. Notice that our conventions differ by a sign from the ones used in [33, 34].

Even though the form factor cannot be computed from first principles, there are certain kinematical limits where theoretical or experimental information is available. For instance, when both photons are on-shell, the form factor is determined (in the chiral limit) solely by the WZW anomaly term

$$F_{\gamma^* \gamma^* \pi^0}(0, 0) = -\frac{N_C}{12\pi^2 f_\pi}, \quad (39)$$

and it is therefore convenient to define

$$F_{\gamma^* \gamma^* \pi^0}(Q_1^2, Q_2^2) = -\frac{N_C}{12\pi^2 f_\pi} K(Q_1^2, Q_2^2), \quad (40)$$

such that $K(0, 0) = 1$.

On the experimental side, studies have focused on the low energy behavior, when one of the photons is exactly on-shell and the other slightly off-shell. In this kinematic regime it is common to define the slope of the anomalous form factor a_π as

$$K(0, Q^2) = K(Q^2, 0) = \left[1 - \frac{a_\pi}{m_\pi^2} Q^2 + \frac{b_\pi}{m_\pi^4} Q^4 \dots \right], \quad (41)$$

i.e.,

$$a_\pi = -m_\pi^2 \left[\frac{dK(Q^2, 0)}{dQ^2} \right]_{Q^2=0}. \quad (42)$$

The world average is presently $a_\pi = 0.032(4)$, mainly driven by the results of the CELLO collaboration [15] on $\pi^0 \rightarrow e^+ e^- \gamma$. Given the importance of this kinematical regime for the evaluation of the $(g-2)_\mu$, we also define the curvature b_π as

$$b_\pi = m_\pi^4 \left[\frac{dK(Q^2, 0)}{dQ^4} \right]_{Q^2=0}. \quad (43)$$

Later on we will use the different holographic models to obtain a determination for both a_π and b_π .

Another source of information comes when one of the photons is on-shell and the other far off-shell. Then the expected behavior of the pion form factor is dictated by the Brodsky-Lepage quark-counting rules [35, 36],

$$\lim_{Q^2 \rightarrow \infty} K(0, Q^2) \sim \frac{1}{Q^2}. \quad (44)$$

Data on this kinematical regime is available from $e^+ e^- \rightarrow e^+ e^- \pi^0$. The behavior of the previous equation is reasonably reproduced by CLEO [37] but incompatible with recent data by BABAR [38]. Hopefully upcoming BABAR data with better statistics will help clarify the situation. While the discrepancy is surprising, we want to emphasize that the kinematical regime we are considering does not accept an OPE expansion, and therefore that Eq. (44) is not on the same footing as a short distance constraint.

Short distance constraints can be obtained when both photons have large and equal virtualities. In this case,

$$\lim_{Q^2 \rightarrow \infty} K(Q^2, Q^2) = \frac{8\pi^2 f_\pi^2}{N_c} \frac{1}{Q^2}. \quad (45)$$

It is worth stressing that all the constraints and experimental information presented above refer to the pion being strictly on-shell. In our case, since we are working in the chiral limit, to a very good approximation $p^2 = m_\pi^2 \sim 0$. We will come back to the on-shellness of the pion when we discuss the pion exchange diagram in $(g-2)_\mu$. For the time being, we will concentrate on the pion form factor as predicted from the different holographic models.

A. Holographic predictions

In terms of holographic QCD, $K(Q_1^2, Q_2^2)$ can be obtained from the VVA terms of the Chern Simons action. Working in the axial gauge, $\mathcal{B}_z = 0$, and gathering the relevant pieces trilinear in the fields one finds:

$$S_{\text{CS}}^{\text{AdS}} = \frac{N_c}{24\pi^2} \epsilon^{\mu\nu\rho\sigma} \text{tr} \int d^4x dz (\partial_z \mathcal{B}_\mu) \left[\mathcal{F}_{\nu\rho} \mathcal{B}_\sigma + \mathcal{B}_\nu \mathcal{F}_{\rho\sigma} \right]. \quad (46)$$

Replacing $A_\mu = \partial_\mu \pi$ and taking the pion to be on-shell one ends up with

$$S_{\text{CS}}^{\text{AdS}} = \frac{N_c}{12\pi^2} \epsilon^{\mu\nu\rho\sigma} \int d^4x \int_0^{z_0} dz \pi^a \times \left[2 \partial_z \beta \partial_\rho V_\mu^a \partial_\sigma \hat{V}_\nu - \beta \partial_z \left(\partial_\rho V_\mu^a \partial_\sigma \hat{V}_\nu \right) \right], \quad (47)$$

where $\beta(z)$ stands for the pion wave function, which we will denote as $\Psi(z)$ or $\alpha(z)$, depending on the model.

Integrating by parts over z in the second term above and dismissing a boundary term (cf. [33]) in order to reproduce the standard four dimensional WZW action one gets

$$S_{\text{CS}}^{\text{AdS}} = \frac{N_c}{4\pi^2} \epsilon^{\mu\nu\rho\sigma} \int_0^{z_0} dz (\partial_z \beta) \int d^4x \pi^a (\partial_\rho V_\mu^a) (\partial_\sigma \hat{V}_\nu). \quad (48)$$

Variation of $S_{\text{CS}}^{\text{AdS}}$ above gives the three-point function:

$$T_{\alpha\mu\nu}(p, q_1, q_2) = \frac{N_c}{12\pi^2} \frac{p_\alpha}{p^2} \epsilon_{\mu\nu\rho\sigma} q_1^\rho q_2^\sigma K(Q_1^2, Q_2^2). \quad (49)$$

In compliance with the large- N_c limit, in extradimensional models the form of the interaction vertex between the pion and two external electromagnetic currents is mediated by the full tower of Kaluza-Klein vector mesons. From the variation of the Chern-Simons action with respect to the external sources one obtains

$$K(Q_1^2, Q_2^2) = - \int_0^{z_0} \mathcal{J}(Q_1, z) \mathcal{J}(Q_2, z) \partial_z \beta(z) dz + (\text{possible boundary terms}), \quad (50)$$

where $\mathcal{J}(Q, z)$ is the vector bulk-to-boundary propagator at Euclidean momentum $Q^2 = -q^2$, defined in the previous section.

The significance of boundary terms in the Chern-Simons action was studied in detail in [28]. In the context of the HW1 model, boundary terms in the expression of $K(Q_1^2, Q_2^2)$ were shown to be needed in order to have the right normalization required by the QCD axial anomaly, namely $K(0, 0) = 1$. The presence of these boundary terms is closely related to the infrared behavior of the pion wave function. As pointed out in Eq. (12), in the HW1 model the value of the pion wave function at z_0 does not cancel and requires the addition of a boundary term [33]

$$K(Q_1^2, Q_2^2) = - \int_0^{z_0} \mathcal{J}(Q_1, z) \mathcal{J}(Q_2, z) \partial_z \Psi(z) dz + \mathcal{J}(Q_1, z_0) \mathcal{J}(Q_2, z_0) \Psi(z_0). \quad (51)$$

No boundary term is needed both in the case of the HW2 and the SS models. The correct normalization is obtained in both cases (using $\mathcal{J}(0, z) = 1$) due to the boundary conditions satisfied by $\alpha(z)$:

$$K(0, 0) = - \int_0^{z_0} \partial_z \alpha(z) dz = \alpha(0) = 1. \quad (52)$$

For the SW models, since the pion wave function is introduced by hand, it depends on the ansatz made. In general, pion wave function that do not cancel at the infrared brane will require boundary terms to correctly implement the axial anomaly in $K(Q_1, Q_2)$.

Equipped with Eqs. (50) and (51), together with the different expressions for the pion wave function and vector bulk-to-boundary propagator, one can easily find the expressions for the pion form factor. We are mostly interested in checking whether short distance constraints are satisfied and to what extent the low energy information complies with experimental data.

B. Large- Q^2 behavior

In asymptotically AdS holographic models, it is easy to show that the function $K(Q_1, Q_2)$ automatically satisfies the high energy constraints discussed in the previous Section. For instance, for arbitrarily large Q_1 and Q_2 , and working in the HW2 model, it is not difficult to show that the general expression

reads

$$\begin{aligned}
K(w, Q^2) &\simeq \frac{2}{z_0^2 Q^2} \sqrt{1-w^2} \\
&\times \int_0^\infty d\xi K_1(\sqrt{1+w\xi}) K_1(\sqrt{1-w\xi}) \xi^3 \\
&\simeq \frac{2}{w^3 z_0^2 Q^2} [w - (1-w^2) \tanh^{-1} w] ,
\end{aligned} \tag{53}$$

where $w = \frac{Q_1^2 - Q_2^2}{2Q^2}$, $2Q^2 = Q_1^2 + Q_2^2$ and $\xi = Qz$.

It is easy to show that the momentum dependence of the previous result also holds for the HW1 and SW models: AdS dictates the large- Q^2 behavior of the bulk-to-boundary propagator, and this is common to all of them. Moreover, the shape of the pion wave function is very similar for all the models close to the ultraviolet boundary, as illustrated in Fig. 2. Indeed, as pointed out in [34], $\alpha(z)$ and the pion wave function (11) coincide in the deep ultraviolet, since at small z

$$\partial_z \Psi(z) \simeq -f_\pi^2 g_5^2 z = -2 \frac{z}{z_0^2} = \partial_z \alpha(z) . \tag{54}$$

Notice that differences between HW1 and HW2 only affect the infrared of the theory, and therefore are of no relevance for the large- Q^2 behavior (at most exponentially suppressed like $\mathcal{O}(e^{-Qz_0})$).

The form of the coefficient in front of Eq. (53) will obviously change depending on the details of the model. For instance, the SW model with the *ad hoc* Gaussian pion wave function is recovered by replacing $z_0 \rightarrow 1/\kappa$. Since z_0 is related to the pion decay constant, while κ is matched to the $\rho(770)$ mass, if we impose numerical agreement between both models we find the relation

$$m_\rho^2 = 8\pi^2 f_\pi^2 , \tag{55}$$

which can be compared for instance with the prediction [39]

$$m_\rho^2 = \frac{16\sqrt{6}}{5} \pi^2 f_\pi^2 , \tag{56}$$

coming from a large- N_c sum rule analysis of Π_{VV} and Π_{AA} . It is reassuring that both predictions are in excellent agreement.

When $Q_1 = Q_2 = Q$, Eq. (53) simplifies to

$$K(Q^2, Q^2) = \frac{4}{3z_0^2 Q^2} . \tag{57}$$

With the expression for z_0 in the HW2 model, $z_0 = 2/g_5^2 f_\pi$, and $g_5^2 = 12\pi^2/N_c$, it is easy to show that it agrees with Eq. (45). Actually one can go even

further to show that the leading terms for $\lambda \rightarrow \infty$ are

$$\begin{aligned}
K(\lambda^2 Q^2, (\lambda^2 Q^2 - P^2)) &\simeq \\
&\frac{2}{3} \frac{g_5^2 f_\pi}{Q^2} \left\{ \frac{1}{\lambda^2} + \frac{1}{\lambda^3} \frac{P \cdot Q}{Q^2} + \mathcal{O}\left(\frac{1}{\lambda^4}\right) \right\} ,
\end{aligned} \tag{58}$$

which, up to $\mathcal{O}(\alpha_S)$ corrections which cannot be captured by the HW2 model, is the short distance behavior found in [4] and [40].

One can also explore the regime where one photon is on-shell and the other far off-shell. In that case,

$$K(0, Q^2) \simeq \frac{2}{z_0^2 Q^2} \int_0^\infty d\xi K_1(\xi) \xi^2 = \frac{4}{z_0^2 Q^2} = \frac{8\pi^2 f_\pi^2}{Q^2} , \tag{59}$$

which displays the Brodsky-Lepage scaling, cf. Eq. (44).

Eqs. (53), (57), (58) and (59) do not hold however for the models without asymptotic AdS metric, *i.e.* the Sakai-Sugimoto and the flat HW2 model. At least for the latter, calculations can be performed analytically with the results

$$\begin{aligned}
K(w, Q^2) &= \frac{1}{2wz_0 Q} \\
&\times [\sqrt{1+w} \tanh(Qz_0 \sqrt{1+w}) - \{w \rightarrow -w\}] , \\
K(Q^2, Q^2) &= \frac{1}{2Qz_0} , \\
K(0, Q^2) &= \frac{1}{Qz_0} ,
\end{aligned} \tag{60}$$

which fail to reproduce the OPE of QCD.

C. Small- Q^2 behavior and predictions for the parameters a_π and b_π

At small virtualities one can expand $K(Q_1^2, Q_2^2)$ in the form

$$\begin{aligned}
K(Q_1^2, Q_2^2) &\simeq 1 + \hat{\alpha} (Q_1^2 + Q_2^2) + \hat{\beta} Q_1^2 Q_2^2 \\
&+ \hat{\gamma} (Q_1^4 + Q_2^4) .
\end{aligned} \tag{61}$$

By comparison with the previous section, we immediately conclude that $a_\pi = -\hat{\alpha} m_\pi^2$, $b_\pi = \hat{\gamma} m_\pi^4$. The parameter $\hat{\beta}$ does not contribute to processes when one of the photons is real. Even so, it will be a useful parameter in the determination of $(g-2)_\mu$ in Section IV.

Eq. (61) can be reproduced from holographic models by working out the small- Q^2 behavior of $\mathcal{J}(Q, z)$, which we will parameterize as

$$\mathcal{J}(Q, z) \equiv 1 - Q^2 g(z) + Q^4 h(z) . \tag{62}$$

| Model | $\hat{\alpha}$ (GeV ⁻²) | $\hat{\beta}$ (GeV ⁻⁴) | $\hat{\gamma}$ (GeV ⁻⁴) |
|------------|-------------------------------------|------------------------------------|-------------------------------------|
| HW1 | -1.60 | 3.01 | 2.63 |
| HW2 (AdS) | -1.81 | 3.65 | 3.06 |
| HW2 (Flat) | -1.37 | 2.25 | 2.25 |
| SS | -2.04 | 4.56 | 3.55 |
| SW | -1.66 | 3.56 | 2.76 |

TABLE I: Values of $\hat{\alpha}$, $\hat{\beta}$ and $\hat{\gamma}$ for the holographic models discussed in the main text.

The functions $g(z), h(z)$ can be easily obtained by solving perturbatively in Q^2 the equation of motion for the different models. This leads to the following analytic expressions:

(i) HW1 and HW2 models:

$$g(z) = \frac{z^2}{4} \left[1 - 2 \log \left(\frac{z}{z_0} \right) \right],$$

$$h(z) = \frac{z^4}{16} \left[2 \left(\frac{z_0}{z} \right)^2 - \frac{5}{4} + \log \left(\frac{z}{z_0} \right) \right]; \quad (63)$$

(ii) SS model:

$$g(z) = M_{KK}^{-2} \left[\int_0^z dy \frac{y}{(\sin y)^{4/3}} + z \int_z^{\pi/2} \frac{dy}{(\sin y)^{4/3}} \right],$$

$$h(z) = M_{KK}^{-2} \left[\int_0^z dy \frac{y g(y)}{(\sin y)^{4/3}} + z \int_z^{\pi/2} dy \frac{g(y)}{(\sin y)^{4/3}} \right]; \quad (64)$$

(iii) SW model:

$$g(z) = -\frac{z^2}{4} \int_0^1 \exp \left[-\frac{x}{1-x} \kappa^2 z^2 \right] \frac{\ln x}{(1-x)^2} dx,$$

$$h(z) = \frac{z^2}{32\kappa^2} \int_0^1 \exp \left[-\frac{x}{1-x} \kappa^2 z^2 \right] \frac{\ln^2 x}{(1-x)^2} dx; \quad (65)$$

(iv) flat case:

$$g(z) = z^2 \left[\frac{z_0}{z} - \frac{1}{2} \right],$$

$$h(z) = \frac{z^4}{24} \left[1 - 4 \frac{z_0}{z} + 8 \left(\frac{z_0}{z} \right)^3 \right]. \quad (66)$$

Plugging the previous expressions into Eq. (50) or (51) one can obtain the different determinations for the low energy parameters. For the HW1 model one

finds

$$\hat{\alpha} = -\frac{z_0^2}{4} \Psi(z_0) + \int_0^{z_0} g(z) \partial_z \Psi(z) dz,$$

$$\hat{\beta} = \frac{3z_0^4}{64} \Psi(z_0) - \int_0^{z_0} h(z) \partial_z \Psi(z) dz,$$

$$\hat{\gamma} = \frac{z_0^4}{16} \Psi(z_0) - \int_0^{z_0} g(z)^2 \partial_z \Psi(z) dz, \quad (67)$$

while for the remaining models:

$$\hat{\alpha} = \int_0^{z_0} g(z) \partial_z \alpha(z) dz,$$

$$\hat{\beta} = -\int_0^{z_0} h(z) \partial_z \alpha(z) dz,$$

$$\hat{\gamma} = -\int_0^{z_0} g(z)^2 \partial_z \alpha(z) dz. \quad (68)$$

The values for the different models are collected in Table I. Experimentally, only the slope has been determined, $\hat{\alpha} = -1.76(22)$ GeV⁻² [41], which is correctly reproduced by the HW1, HW2 and SW models. Notice that, even though the slope is a genuine low energy quantity, models without asymptotic AdS metric fail to reproduce the experimental value. The quartic parameters $\hat{\beta}$ and $\hat{\gamma}$, using the phenomenologically acceptable HW1, HW2 and SW models, are predicted to be $\hat{\beta} = 3.33(32)$ GeV⁻⁴ and $\hat{\gamma} = 2.84(21)$ GeV⁻⁴. With higher statistics on the experimental side, the holographic prediction for $\hat{\gamma}$ can be tested. Both holographic predictions will be used in the evaluation of the hadronic light-by-light contribution of the $(g-2)_\mu$.

Before moving to the evaluation of the $(g-2)_\mu$, it is important to explore the resonance contributions to the results of table 1. For this, we write the vector bulk-to-boundary propagator in its spectral decomposition

$$\mathcal{J}(z, Q) = \sum_{n=1}^{\infty} \frac{f_n}{Q^2 + m_n^2} \psi_n(z), \quad (69)$$

where m_n is the mass of the n th vector resonance and f_n is related to its decay constant. Plugging this expression into Eq. (50), one obtains the double series

$$K(Q_1^2, Q_2^2) \equiv \sum_{k,l=1}^{\infty} \frac{B_{kl}}{(Q_1^2 + m_k^2)(Q_2^2 + m_l^2)}. \quad (70)$$

This expression is of the form expected in the large- N_c limit, with the full tower of vector mesons propagating between the pion and the two photons. The contributions for $\hat{\alpha}$, $\hat{\beta}$ and $\hat{\gamma}$ from the first three vector radial excitations are reported in Table II. The important point to notice is that lowest vector

| Model | $\hat{\alpha}_n/\hat{\alpha}$ | | | $\hat{\beta}_n/\hat{\beta}$ | | | $\hat{\gamma}_n/\hat{\gamma}$ | | |
|------------|-------------------------------|-------|-------|-----------------------------|-------|------|-------------------------------|-------|------|
| HW1 | 1.20 | -0.18 | -0.04 | 1.10 | -0.06 | 0.01 | 1.20 | -0.22 | 0.06 |
| HW2 (AdS) | 1.30 | -0.37 | 0.06 | 1.10 | -0.11 | 0.01 | 1.30 | -0.37 | 0.08 |
| HW2 (flat) | 0.99 | 0.01 | 0.00 | 1.00 | 0.00 | 0.00 | 1.00 | 0.00 | 0.00 |
| SS | 1.70 | -1.10 | 0.49 | 1.30 | -0.34 | 0.07 | 1.60 | -1.10 | 0.54 |
| SW | 0.75 | 0.14 | 0.05 | 0.87 | 0.09 | 0.02 | 0.88 | 0.09 | 0.02 |

TABLE II: Contribution to $\hat{\alpha}$, $\hat{\beta}$ and $\hat{\gamma}$ due to the first three vector meson radial excitations. For $\hat{\alpha}_n$, each sub-column ($n = 1, 2, 3$) contains the contribution of $k, l \leq n$ terms. $\hat{\beta}_n$ and $\hat{\gamma}_n$ are defined analogously.

dominance is a feature common to all models (from the practically ρ -dominance of the flat model to the more moderate behavior of the SS model). Incidentally, notice also that with the exception of the SW model, the contribution of the first resonance tends to overshoot the total value, and has to be compensated by negative contributions from higher order resonances. Finally, let us remark that the representation of Eq. (70) is only reliable for moderate values of the resonance indices. Most likely Eq. (70) is at most an asymptotic expansion, and therefore beyond a certain threshold it ceases to be meaningful.

IV. THE HADRONIC LIGHT BY LIGHT CONTRIBUTION TO THE $(g - 2)_\mu$

With experimental accuracies at the 10^{-10} level, precise determinations of the hadronic light-by-light contribution to the $(g - 2)_\mu$ become of paramount importance. The problem is that genuine nonperturbative techniques are required and having theoretical uncertainties under control is certainly a challenging task. The hadronic light-by-light contribution to the $(g - 2)_\mu$ is depicted in Fig. 3. When internal momenta in the loop are high enough one can use perturbation theory, but a proper evaluation also requires low energies, *i.e.* Goldstone bosons and hadrons. The neutral pion exchange contribution, depicted in Fig 4, turns out to be the dominant piece ($a_\mu^{(\pi^0)} \sim 7 \cdot 10^{-10}$) followed by the η and η' contributions ($a_\mu^{(\eta, \eta')} \sim 3 \cdot 10^{-10}$). Quark and Goldstone loops, axial vectors and scalars are also expected to contribute at the level of $(1 - 2) \cdot 10^{-10}$, but cancellations occur (scalars and Goldstone loops contribute negatively) and so the Goldstone boson exchange ends up collecting the bulk of the effect. In particular this means that the naive large- N_c counting works and single exchange resonances are the dominant effect. This observation suggests that procedures based on the $1/N_c$ framework are suitable tools to address the problem.

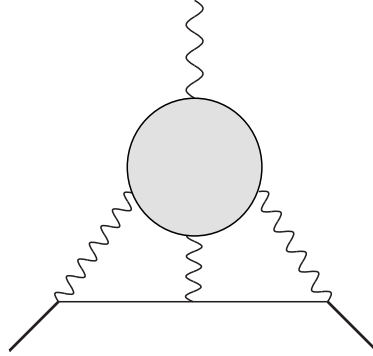


FIG. 3: Hadronic light by light contribution to $(g - 2)_\mu$.

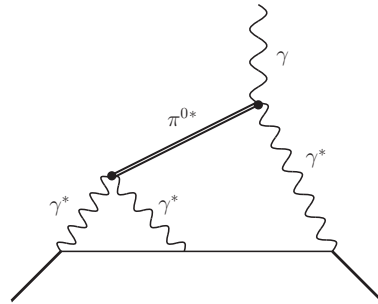


FIG. 4: One of the diagrams contributing to pion exchange in the hadronic light by light contribution to $(g - 2)_\mu$.

Different parameterizations have been used in the past to evaluate the hadronic light-by-light contribution. In particular, there is the detailed study of [4] with different parameterizations based on lowest meson dominance (LMD). Having in mind what we did so far, one could be tempted to use the results of the previous Section on the pion form factor and use them to evaluate each of the $\pi^0 \gamma \gamma$ vertices of the diagram in Fig. 4, as has been recently done for the HW1 model [42]. However, notice that momentum conservation forces the pion to be off-shell. Therefore, the kinematical regimes which are relevant for the hadronic light by light contribution preclude the use of the pion form factor.

We are thus forced to resort to a different method to evaluate the diagram of Fig. 4. The strategy we will follow is to suggest an ansatz for the form factor and determine its free parameters by demanding that, when the pion goes on-shell, it satisfies the known theoretical and experimental constraints. Additionally, when the pion is highly off-shell, we will impose the short distance constraint discussed in Ref. [6]. The results we found for holographic models in the previous section will also be used as

additional input, such that we will be able to play simultaneously with experimental, QCD short distance and holographic constraints.

The parameterization we will use is the following:

$$K(q_1^2, q_2^2) = 1 + \lambda \left(\frac{q_1^2}{q_1^2 - m_V^2} + \frac{q_2^2}{q_2^2 - m_V^2} \right) + \eta \frac{q_1^2 q_2^2}{(q_1^2 - m_V^2)(q_2^2 - m_V^2)}, \quad (71)$$

first introduced in the study of $K_L \rightarrow \mu^+ \mu^-$ decays [18]. This parameterization was originally suggested to parameterize the low energy slope of three point functions, and has been used in experimental studies of $K_L \rightarrow \mu^+ \mu^-$ and $K_L \rightarrow \pi^0 e^+ e^-$. Here we want to exploit it fully and promote it to an analytic interpolator valid at all energies.

Aside from being simple and with a very intuitive low energy behavior, the previous parameterization has additional advantages. In Ref. [4] it was shown that in the general two-loop expression for the pion contribution to the hadronic light-by-light scattering all angular integrations can be performed using the hyperspherical approach if the interpolator can be cast in the generic form:

$$F_{\pi^0 \gamma^* \gamma^*}(q_1^2, q_2^2) = -\frac{N_c}{12\pi^2 f_\pi} \left[f(q_1^2) - \sum_i \frac{1}{q_2^2 - m_i^2} g_i(q_1^2) \right]. \quad (72)$$

The diagram of Fig. 4 can then be evaluated through

the following expression:

$$a_\mu^{\pi^0} = \left(\frac{\alpha_{em}}{\pi} \right)^3 \left\{ a_{\mu(1)}^{\pi^0} + a_{\mu(2)}^{\pi^0} \right\}, \quad (73)$$

where

$$a_{\mu(1)}^{\pi^0} = \int_0^\infty dQ_1 \int_0^\infty dQ_2 \left[w_1(Q_1, Q_2) G_1(Q_1, Q_2) + w_2(m_V, Q_1, Q_2) G_2(Q_1, Q_2) \right] \quad (74)$$

and

$$a_{\mu(2)}^{\pi^0} = \int_0^\infty dQ_1 \int_0^\infty dQ_2 \left[w_3(m_V, Q_1, Q_2) G_3(Q_1, Q_2) + w_3(m_\pi, Q_1, Q_2) G_4(Q_1, Q_2) \right]. \quad (75)$$

G_i are generalized form factors whose expressions are given by

$$\begin{aligned} G_1(x, y) &= -\frac{N_c}{12\pi^2 f_\pi} f(-x^2) F_{\pi^0 \gamma^* \gamma^*}(-y^2, 0), \\ G_2(x, y) &= -\frac{N_c}{12\pi^2 f_\pi} \frac{g(-x^2)}{m_V^2} F_{\pi^0 \gamma^* \gamma^*}(-y^2, 0), \\ G_3(x, y) &= -\frac{N_c}{12\pi^2 f_\pi} \frac{g(0)}{m_\pi^2 - m_V^2} F_{\pi^0 \gamma^* \gamma^*}(-x^2, -y^2), \\ G_4(x, y) &= -\frac{N_c}{12\pi^2 f_\pi} f(0) F_{\pi^0 \gamma^* \gamma^*}(-x^2, -y^2) - G_3(x, y), \end{aligned} \quad (76)$$

and the weight factors w_i take the form

$$\begin{aligned} w_1(x, y) &= \frac{\pi^2}{6m_\mu^2 xy(y^2 + m_\pi^2)} \left[4(y^2 - 2m_\mu^2)(x^2 - y^2)^2 \log(1 + \lambda(0, x, y)) \right. \\ &+ \left((x^6 + y^6) - x^2 y^4 - 3x^4 y^2 + \frac{x^4 y^6}{2m_\mu^4} - \frac{x^4 y^4}{m_\mu^2} - 4m_\mu^2 x^2 y^2 - (x^2 - y^2)^2 \eta_0 \right) \left(1 - \frac{\xi(x)}{x^2} \right) \\ &+ \left. y^2(y^4 - 4m_\mu^4) \frac{\xi(x)}{m_\mu^2} - x^4(y^2 - 2m_\mu^2)^2 \frac{\xi(y)}{2m_\mu^4} + (y^2 - 2m_\mu^2)(x^2 y^2 - 2m_\mu^2(x^2 + y^2)) \frac{\xi(x)\xi(y)}{2m_\mu^4} \right], \quad (77) \end{aligned}$$

$$\begin{aligned} w_2(m, x, y) &= \frac{\pi^2}{6m_\mu^2 xy(y^2 + m_\pi^2)} \left[4(y^2 - 2m_\mu^2)(x^2 - y^2)^2 \log(1 + \lambda(0, x, y)) \right. \\ &- 4(y^2 - 2m_\mu^2)(m^4 + (x^2 - y^2)^2 + 2m^2(x^2 + y^2)) \log(1 + \lambda(m, x, y)) \\ &+ \left\{ (m^4 + 2m^2(x^2 + y^2) + (x^4 + y^4) - 2x^2 y^2) \eta_m - (x^2 - y^2)^2 \eta_0 - \frac{m^2}{m_\mu^2} x^2 (y^2 - 2m_\mu^2) \xi(y) \right. \\ &+ \left. \left. \frac{m^2}{m_\mu^2} x^2 y^4 - m^6 - 3m^4(x^2 + y^2) - 3m^2(x^4 + y^4) - 2m^2 x^2 y^2 \right\} \left(1 - \frac{\xi(x)}{x^2} \right) \right], \quad (78) \end{aligned}$$

$$\begin{aligned}
w_3(m, x, y) = & \frac{\pi^2}{6m_\mu^2 xy} [4(x^2 - y^2)(m_\mu^2(y^2 - x^2) + 2x^2 y^2) \log(1 + \lambda(0, x, y)) + 4 \log(1 + \lambda(m, x, y)) \\
& \times (m^4 m_\mu^2 + (x^2 - y^2)(m_\mu^2(x^2 - y^2) - 2x^2 y^2) + 2m^2(m_\mu^2(x^2 + y^2) + x^2 y^2)) + m^4(x^2 + y^2) \\
& + 2m^2(x^4 + y^4) - m^2 x^2 y^2 - m^2(m^2 + 2x^2 + y^2)\xi(x) - m^2(m^2 - 3x^2 + 2y^2)\xi(y) - m^2 \xi(x)\xi(y) \\
& + \{(x^2 + y^2)\eta_0 - (m^2 + x^2 + y^2)\eta_m\}(x^2 - \xi(x)) + \{(y^2 - 3x^2)\eta_0 - (m^2 + y^2 - 3x^2)\eta_m\}(y^2 - \xi(y))] .
\end{aligned} \tag{79}$$

In the previous expressions we have defined

$$\lambda(m, x, y) = \frac{(m^2 + x^2 + y^2 - \eta_m)(x^2 - \xi(x))(y^2 - \xi(y))}{8m_\mu^2 x^2 y^2} \tag{80}$$

$$\eta_m = \sqrt{(m^2 + x^2 + y^2)^2 - 4x^2 y^2} , \tag{81}$$

and

$$\xi(z) = \sqrt{z^4 + 4m_\mu^2 z^2} . \tag{82}$$

In other words, the contribution to the $(g - 2)_\mu$ can be reduced to a more tractable double integral, that at least can be evaluated numerically.

It is not difficult to verify that the interpolator of Eq. (71) is of the form (72) with

$$f(q^2) = 1 + \lambda + (\lambda + \eta) \frac{q^2}{q^2 - m_V^2} , \tag{83}$$

$$g_V(q^2) = -m_V^2 \left[\lambda + \eta \frac{q^2}{q^2 - m_V^2} \right] . \tag{84}$$

Notice that the interpolator of Eq. (71) is assumed not to depend on the pion momentum. This simplifying assumption, together with the specific form of Eq. (72), is crucial to be able to use Eqs. (74) and (75).

Our parameterization has 3 free parameters, λ , η and m_V . In lowest meson dominance models it is common to identify $m_V \equiv m_\rho$. This strategy might be reasonable when little information about the correlator is known and the interpolator is underconstrained. This is however not the case here and we think it more appropriate to take full advantage of the constraints. Therefore, we will let m_V be set by the constraints. From a more formal point of view, the interpolator we are using is mathematically known as a Pade approximant, which is the natural interpolator in models at leading order in the $1/N_c$ expansion. If constraints on different energy regimes are imposed, the interpolator is called a multi-point Pade approximant. While the number of low and high energy constraints to be imposed depends on the problem at hand, experience recommends that stability is optimized when both high and low energy constraints play a role. Finally,

one distinguishes between a Pade-type and a plain Pade approximant, depending on whether the poles of the interpolator are fixed by hand from the start or determined through the constraints. We will here follow the latter strategy.

As a reference exercise we will impose the following constraints:

$$1 + 2\lambda + \eta = 0 , \tag{85}$$

$$\lambda + \eta = -\frac{4\pi^2 f_\pi^2}{3m_V^2} , \tag{86}$$

$$\frac{\lambda}{m_V^2} = (-1.76 \pm 0.22) \text{ GeV}^{-2} . \tag{87}$$

The first two are short distance information, namely the requirement that $K(Q^2, Q^2)$ at high energies does not go like a constant (first equation) and that its $1/Q^2$ behavior has the right coefficient (see Eq. (45), with $N_c = 3$). The last equation is the experimental constraint on the slope of the pion form factor. Using as input parameters

$$\begin{aligned}
m_\mu &= 105.658367(4) \text{ MeV} , \\
m_\pi &= 134.9766(6) \text{ MeV} , \\
f_\pi &= 92.4 \text{ MeV} , \\
\alpha_{em} &= 1/137.03599976 ,
\end{aligned} \tag{88}$$

the parameters of the model become

$$\begin{aligned}
\lambda &= -0.73 \pm 0.05 , \\
\eta &= 0.46_{-0.13}^{+0.10} , \\
m_V &= 0.64_{-0.06}^{+0.07} \text{ GeV} ,
\end{aligned} \tag{89}$$

where the uncertainties are due to the experimental error bars on the slope. With these values, the prediction for the anomalous magnetic moment is

$$a_\mu^{\pi^0} = 6.7(3) \cdot 10^{-10} . \tag{90}$$

In Table III the comparison is made with the LMD result quoted in Ref. [4]. We see that the contributions for the different integrals are in very good agreement. Note that this agreement happens even though $m_V = 0.64 \text{ GeV} \neq m_\rho$ and the interpolators are very different in nature. The value we find for the mass scale has to be interpreted as an effective

| Model | $w_1 G_1$ | $w_2 G_2$ | $w_3 G_3$ | $w_4 G_4$ | a_μ |
|-----------------------|-----------|-----------|-----------|-----------|-------------------------|
| LMD | +0.015 | +0.042 | +0.0016 | -0.0002 | $7.3 \cdot 10^{-10}$ |
| DIP $_{\hat{\alpha}}$ | +0.018(3) | +0.034(4) | +0.0016 | -0.0002 | $6.7(3) \cdot 10^{-10}$ |
| DIP $_{m_\rho}$ | +0.015 | +0.043 | +0.0016 | -0.0002 | $7.35 \cdot 10^{-10}$ |

TABLE III: Determination of a_μ with the DIP parameterisation and comparison with the LMD model. We explicitly show the contribution from the different generalized form factors G_i .

measure of the relevant scale for the problem. Therefore, we confirm that m_ρ is indeed very close to the natural scale to estimate the pion exchange. This observation agrees with the results presented in Table III in the previous section for the different holographic models. In other words, the LMD observed in $(g-2)_\mu$ is a consequence of LMD in the anomalous pion electromagnetic form factor, a feature that holographic realizations successfully predict. A natural consequence of it all is that the curvature of the pion form factor can be estimated as

$$\hat{\gamma} = -\frac{\hat{\alpha}}{m_V^2} \sim 2.97 \text{ GeV}^{-4}, \quad (91)$$

which agrees with the holographic prediction.

In the third line of Table III we have repeated our determination of a_μ , but instead of fixing the slope we set $m_V = m_\rho$. Notice that now we recover the results of LMD, even though the interpolators are very different. Thus, the difference between LMD and our approach are entirely due to the choice of mass scale, which in our case is determined self-consistently. We also observe that the bulk of the determination comes from $a_{\mu(1)}^{\pi^0}$, while the (subleading) contributions to $a_{\mu(2)}^{\pi^0}$ are rather insensitive to the variation of input parameters or constraints.

In Fig. 5 we show the shape of the weight functions entering the dominant $a_{\mu(1)}^{\pi^0}$. As pointed out in [4], the relevant contributions are highly peaked at low values of momenta, $0 \sim Q^2 \sim 0.5 \text{ GeV}$. This suggests that more information on low energies can help improve the determination of a_μ . However, at the same time one still needs to ensure the short distance constraints. More sophisticated interpolators are therefore needed. In the following we will refine our analysis by generalising the DIP parameterisation.

A. Extensions of the DIP ansatz

The simplest extension of the DIP parameterisation compatible with the general form of Eq. (72) is

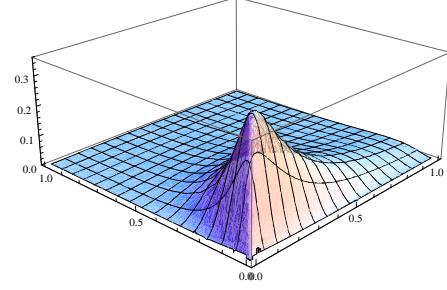


FIG. 5: The integrand of Eq. (74).

to increase the number of poles, *i.e.*,

$$K(q_1, q_2) = 1 + \sum_i^2 \lambda_i \left(\frac{q_1^2}{q_1^2 - m_i^2} + \frac{q_2^2}{q_2^2 - m_i^2} \right) + \sum_i^2 \eta_i \frac{q_1^2 q_2^2}{(q_1^2 - m_i^2)(q_2^2 - m_i^2)}, \quad (92)$$

which is the generalised version of Eq. (71). Then one can write accordingly:

$$f(q^2) = 1 + \sum_i^2 \lambda_i + \sum_i^2 (\lambda_i + \eta_i) \frac{q^2}{q^2 - m_i^2}, \quad (93)$$

$$g_i(q^2) = -m_i^2 \left[\lambda_i + \eta_i \frac{q^2}{q^2 - m_i^2} \right]. \quad (94)$$

For our purposes we will consider the following particular cases:

$$K_{(1)}(q_1, q_2) = 1 + \lambda \left(\frac{q_1^2}{q_1^2 - m_1^2} + \frac{q_2^2}{q_2^2 - m_1^2} \right) + \sum_i^2 \eta_i \frac{q_1^2 q_2^2}{(q_1^2 - m_i^2)(q_2^2 - m_i^2)}, \quad (95)$$

and

$$K_{(2)}(q_1, q_2) = 1 + \sum_i^2 \lambda_i \left(\frac{q_1^2}{q_1^2 - m_i^2} + \frac{q_2^2}{q_2^2 - m_i^2} \right) + \eta \frac{q_1^2 q_2^2}{(q_1^2 - m_1^2)(q_2^2 - m_1^2)}. \quad (96)$$

The advantage of dealing with two generalized expressions is that we will be able to assess the dependence of our results on the specific form of the interpolator.

The constraints we will impose now are the following:

(a) Long distance constraints:

$$\sum_i^2 \frac{\lambda_i}{m_i^2} = (-1.76 \pm 0.22) \text{ GeV}^{-2}, \text{ (exp.)} \quad (97)$$

$$\sum_i^2 \frac{\eta_i}{m_i^4} = (3.33 \pm 0.32) \text{ GeV}^{-4}, \text{ (pred.)} \quad (98)$$

$$\sum_i^2 \frac{\lambda_i}{m_i^4} = (-2.84 \pm 0.21) \text{ GeV}^{-4}, \text{ (pred.)} \quad (99)$$

which correspond to the low energy parameters $\hat{\alpha}$, $\hat{\beta}$ and $\hat{\gamma}$ defined in the previous Section. The value for $\hat{\alpha}$ is taken from experiment, while $\hat{\beta}$ and $\hat{\gamma}$ are estimated from the spread of values predicted by the HW1, HW2 and SW models.

(b) Short distance constraints:

$$1 + 2 \sum_i^2 \lambda_i + \sum_i^2 \eta_i = 0, \quad (100)$$

$$\sum_i^2 m_i^2 (\lambda_i + \eta_i) = -\frac{4\pi^2 f_\pi^2}{3}, \quad (101)$$

$$1 + \sum_i^2 \lambda_i = \frac{4\pi^2 f_\pi^2}{3} \chi_0. \quad (102)$$

The first two are the ones already discussed in the previous Sections, namely the absence of constant terms and the matching of the $1/Q^2$ coefficient. The last one comes from the relation [40]

$$\lim_{Q^2 \rightarrow \infty} F_{\pi^0 \gamma^* \gamma^*}(Q^2, 0) = -\frac{f_\pi}{3} \chi_0 + \dots, \quad (103)$$

where one photon is on-shell and the other highly off-shell.

The difference with Eq. (44) is that now the pion is also off-shell. As discussed in [6] this is the relevant kinematical regime for the $(g-2)_\mu$, as can be easily understood from the momentum flow in Fig. 4. As we already discussed above, the off-shellness of the pion precludes the use of the anomalous pion form factor to evaluate the diagram of Fig. 4. Results based on the HW1 model exist [42], but strictly speaking they should be deemed as inconsistent. This was one of the motivations to use the DIP ansatz in our analysis. Indeed, notice that the DIP ansatz has the right kinematics to comply with Eq. (103), which is highly non-trivial.

We want to note at this point that Eq. (103) and the Brodsky-Lepage constraint of Eq. (44), which only differ on the pion being on-shell or off-shell,

cannot be satisfied simultaneously by the different DIP ansätze we have been using. The reason is that, by construction, the DIP interpolator does not depend on the pion momentum. Here we enforce the off-shell condition over the on-shell one for several reasons. First, based on the latest BABAR analysis of $F_{\pi^0 \gamma^* \gamma^*}$, it is unclear at this point whether the Brodsky-Lepage constraint holds or not. Second, the kernel entering $(g-2)_\mu$ is peaked at low energies (see Fig. 5). Accordingly, one would naturally expect the high energy region to have a negligible impact on the anomalous magnetic moment. In this respect, it is quite reassuring that our analysis, in which the $F_{\pi^0 \gamma^* \gamma^*}$ low-energy region is approximately captured by Eqs. (97)-(99), turns out to be in very good agreement with analyses that comply with the Brodsky-Lepage constraint [4, 6]. Finally, the impact of χ_0 was never fully assessed in previous analyses of $(g-2)_\mu$ and, as we will see, it turns out to be a sizeable source of uncertainty.

The main problem with Eq. (103) is that, despite numerous efforts, the parameter χ_0 is only poorly known. Since it cannot be accessed experimentally, one has to resort to non-perturbative techniques to estimate it. However, the different estimates available show strong discrepancies: while recent results based on QCD sum rules [43] or exclusive B decays [44] seem to favor values hovering around $\chi_0 \sim 2-4 \text{ GeV}^{-2}$, estimations based on the axial anomaly [45, 46], Padé approximants [47] or the original sum rule determination of [48] point at much higher values, $\chi_0 \sim 8-11 \text{ GeV}^{-2}$. A recent result in the context of holographic QCD [49] also pointed out the possibility that $\chi_0 \sim 0$. Most of these estimates are given without reference to the renormalization scale. However, its low energy scale evolution was studied in [50] and does not account for the discrepancies found.

With the parameterisations $K_{(1)}$ and $K_{(2)}$ we now have five parameters and six constraints, Eqs. (97) to (102). In principle we could use any five constraints to determine the parameters. However, since the constraints are nonlinear, in any combination of constraints there are in general multiple solutions for the parameters. The only sensible solutions are those that give real parameters and positive masses m_i . However, in most of the cases such solutions do not exist, *e.g.* when one uses Eqs. (97) to (101). For those cases, and in order to always ensure a solution, we will set $m_2 = m_\rho = 0.775 \text{ GeV}$. Therefore, in those cases we will be using four constraints: Eqs. (97), (100) and either (98) or (99). Having seen in the previous Section that m_ρ is a natural scale for the problem, we expect our results to be solid. Actually, in those very few cases when a solution exists, $m_i \sim m_\rho$ and the results are compatible.

| Model | $w_1 G_1$ | $w_2 G_2$ | $w_3 G_3$ | $w_4 G_4$ | a_μ |
|--------------------------------------------------|------------------|------------------|--------------------|-----------|-------------------------------|
| DIP $_{\hat{\alpha}}$ | +0.018(3) | +0.034(4) | +0.0016 | −0.0002 | $6.7(3) \cdot 10^{-10}$ |
| DIP $_{\hat{\beta}; m_2=m_\rho}^{(1)}$ | +0.014 | +0.037 | +0.0015 | −0.0002 | $6.52(15)(10) \cdot 10^{-10}$ |
| DIP $_{\hat{\beta}; m_2=m_\rho}^{(2)}$ | +0.014 | +0.037 | +0.0015 | −0.0002 | $6.55(21)(6) \cdot 10^{-10}$ |
| DIP $_{\hat{\gamma}; m_2=m_\rho}^{(1)}$ | +0.004 | +0.047 | +0.0015 | −0.0002 | $6.09(81)(9) \cdot 10^{-10}$ |
| DIP $_{\hat{\gamma}; m_2=m_\rho}^{(2)}$ | +0.002 | +0.047 | +0.0015 | −0.0002 | $6.21(77)(7) \cdot 10^{-10}$ |
| DIP $_{\hat{\beta}; 0 < \chi_0 < 8.9}^{(1)}$ | [+0.003; +0.047] | [+0.043; +0.022] | [+0.0015; +0.0016] | −0.0002 | $[5.9; 8.9] \cdot 10^{-10}$ |
| DIP $_{\hat{\beta}; 0 < \chi_0 < 4.4}^{(2)}$ | [+0.002; +0.027] | [+0.044; +0.025] | +0.0015 | −0.0002 | $[6.0; 6.7] \cdot 10^{-10}$ |
| DIP $_{\hat{\gamma}; 0 < \chi_0 \leq 6.4}^{(2)}$ | [+0.006; +0.035] | [+0.043; +0.022] | [+0.0015; +0.0016] | −0.0002 | $[6.3; 7.3] \cdot 10^{-10}$ |

TABLE IV: Determination of a_μ with the generalised DIP parameterisations and their comparison with the DIP model. We explicitly show the contribution from the different generalized form factors G_i . The errors in parenthesis are the ones induced by $\hat{\alpha}$ and $\hat{\beta}$ or $\hat{\gamma}$. For the last 3 cases, where χ_0 is inside a range, we show the values for the endpoints.

| Model | $\hat{\alpha}$ (GeV $^{-2}$) | $\hat{\beta}$ (GeV $^{-4}$) | $\hat{\gamma}$ (GeV $^{-4}$) | χ_0 (GeV $^{-2}$) |
|-------------------------------------|-------------------------------|------------------------------|-------------------------------|-------------------------|
| DIP $_{\hat{\alpha}}$ | −1.76* | 2.67 | 4.25 | 2.42 |
| DIP $_{m_\rho}$ | −1.35 | 1.73 | 2.25 | 1.66 |
| DIP $_{\hat{\beta}}^{(1)}$ | −1.76* | 3.33* | 3.78 | 1.61 |
| DIP $_{\hat{\beta}}^{(2)}$ | −1.76* | 3.33* | 3.88 | 1.69 |
| DIP $_{\hat{\gamma}}^{(1)}$ | −1.76* | 4.56 | 2.84* | −0.81 |
| DIP $_{\hat{\gamma}}^{(2)}$ | −1.76* | 5.23 | 2.84* | −0.74 |
| DIP $_{\hat{\beta}, \chi_0}^{(1)}$ | −1.76* | 3.33* | [3.10; −5 · 10 5] | [0; 8.9]* |
| DIP $_{\hat{\beta}, \chi_0}^{(2)}$ | −1.76* | 3.33* | [3.19; −3.18] | [0; 4.4]* |
| DIP $_{\hat{\gamma}, \chi_0}^{(2)}$ | −1.76* | [5.47, −18] | 2.84* | [0; 6.4]* |

TABLE V: Predicted low energy parameters from the different parameterisations. Asterisk quantities are input. Notice from the last three lines that large values for χ_0 are clearly disfavored.

Incidentally, it is by no means trivial that the system of constraints has a solution at all. It crucially depends on the interpolator. In this respect, let us point out that Eq. (100) is satisfied to a very good approximation by the low energy values predicted by the holographic models discussed in the previous Section. Using lowest vector dominance and setting $m_V \sim m_\rho$, one finds

$$\hat{\beta} = -\frac{2m_V^2 \hat{\alpha} + 1}{m_V^4} \sim 3.10 \text{ GeV}^{-4}, \quad (104)$$

which agrees well with Eq. (98) above. This compatibility between long and short distances is of considerable importance. For instance, it opens up a way to estimate $\hat{\beta}$ in $K_L \rightarrow (\mu^+ \mu^-, \pi^0 e^+ e^-)$.

In Table IV we have collected the different predictions for the pion contribution to the hadronic light-by-light using both $K_{(1)}$ and $K_{(2)}$ subject to different subsets of constraints. Eqs. (97), (100) and (101) are always imposed and the subscript on each model indicates which extra constraints were chosen. For completeness, the predicted values for the remaining constraints are collected in Table V.

Let us consider the first five rows of Table IV. From the results we see that the different determinations agree within errors. A conservative estimate including those determinations would give

$$a_\mu = 6.4(5) \cdot 10^{-10}. \quad (105)$$

The dependence on the parameterisation turns out to be very mild. Notice also that both parameterisations tend to follow similar patterns. For instance, the main source of uncertainty always comes from the slope $\hat{\alpha}$, while the effect of $\hat{\beta}$ or $\hat{\gamma}$ is subleading. Thus, an improvement of the CELLO data on the slope of the $\pi^0 \gamma \gamma$ form factor can help decrease the theoretical uncertainty on the hadronic light-by-light.

The previous estimate for a_μ probably overestimates the uncertainty. Notice that the results for DIP $_{\hat{\gamma}}^{(1,2)}$ give lower values of a_μ and with bigger uncertainties. This might be a consequence of the strong correlation between $\hat{\alpha}$ and $\hat{\gamma}$ in the interpolator we are using, and therefore such an uncertainty might be misleading. Additionally, by looking at Table V, we see that DIP $_{\hat{\gamma}}^{(1,2)}$ predicts negative central

values for χ_0 , therefore confirming that the results of $\text{DIP}_{\hat{\gamma}}^{(1,2)}$ might be unreliable. Relying on $\text{DIP}_{\hat{\beta}}^{(1,2)}$ only, our final estimate is

$$a_\mu = 6.54(25) \cdot 10^{-10} . \quad (106)$$

The previous result does not include the uncertainty due to χ_0 . This issue is addressed in the last three lines of Table IV, where we scanned the solution over a wide interval for χ_0 , mostly covering all the values quoted in the literature so far. As can be seen in Table V, large values for χ_0 give wrong predictions for the low energy parameters and hence they are disfavored. While this might be indicative, it is certainly not conclusive. The problem is that given the present confusion around χ_0 , its impact might amount up to a 10%-15% uncertainty in the final estimate for the hadronic light by light contribution to $(g-2)_\mu$. It is therefore essential to have a better understanding of χ_0 .

V. CONCLUSIONS

The muon anomalous magnetic moment is one of the most precisely measured quantities in particle physics, and thus a key parameter to test the appearance of physics beyond the Standard Model. With experimental accuracies expected to reach soon the 10^{-10} level, it is essential to have the theoretical uncertainties in the hadronic light-by-light scattering contribution well under control.

In this paper we have reassessed the pion exchange contribution taking into account constraints on the $\pi^0\gamma\gamma$ form factor at low and high energies. At low energies, when the photons are on-shell, the form factor is determined by the axial anomaly. Experimentally, the slope of the form factor at small virtualities $\hat{\alpha}$ is also known. In order to provide more information at low energies we have used the predictions of holographic models of QCD. To be more precise, we have performed a systematic study of the low energy behavior of $\pi^0\gamma\gamma$ using five different holographic models. The predictions for the quartic parameters $\hat{\beta}$ and $\hat{\gamma}$ were performed with those models that complied with the experimental value for $\hat{\alpha}$.

Information is also provided at large Euclidean momenta. Short distance constraints coming from the OPE of $\pi^0\gamma^*\gamma^*$ have been used, but also the one coming from $(\pi^0)^*\gamma^*\gamma^*$, recently emphasized in [6]. In order to study the sensitivity of $(g-2)_\mu$ to the different constraints we have used a parameterisation for the form factor inspired in the one introduced in [18] to study the low energies of kaon decays.

Our final number for (pion exchange) hadronic

light by light contribution is

$$a_\mu^{\pi^0} = (6.54 \pm 0.25) \cdot 10^{-10} , \quad (107)$$

a result which is a bit lower than the ones reported in LMD models. We have shown that this originates from different choices of the effective mass scale: while LMD assumes $m_V = m_\rho$, in our approach the mass is determined from the matching conditions, with typical values $m_V \sim 640$ MeV slightly lower than m_ρ .

The reported uncertainty is dominated by the experimental accuracy on the slope of $F_{\pi^0\gamma^*\gamma^*}$. The effects of model dependence are evaluated in our approach in two ways: first, through the spread of values for the low energy quartic terms in $F_{\pi^0\gamma^*\gamma^*}$, coming from the different holographic models; and second, using different versions for the parameterisation of $F_{\pi^0\gamma^*\gamma^*}$. The resulting uncertainties are negligible, as it can be seen in Table IV. In view of this, it would be interesting to reduce the experimental uncertainty on $\hat{\alpha}$ and check the holographic predictions on the quartic terms. This is something that could be realistically achieved at DAΦNE with the recent KLOE-2 proposal [11]. Regarding the quartic terms, it is worth noting that both LMD and different versions of the DIP parameterisation tend to predict values for the quadratic terms that are compatible with the holographic predictions. Actually, we have shown that estimates of these parameters can be given, to a remarkable accuracy, in terms of the slope $\hat{\alpha}$:

$$\begin{aligned} \hat{\beta} &= -\frac{2m_V^2\hat{\alpha} + 1}{m_V^4} \sim 3.10 \text{ GeV}^{-4} , \\ \hat{\gamma} &= -\frac{\hat{\alpha}}{m_V^2} \sim 2.97 \text{ GeV}^{-4} . \end{aligned} \quad (108)$$

The previous results are mostly based on ρ -dominance. We therefore conjecture that they be used more broadly, not just in $\pi^0 \rightarrow \gamma\gamma$ but also in the kaon decays $K_L \rightarrow \mu^+\mu^-$ and $K_L \rightarrow \pi^0 e^+ e^-$.

Finally, we want to point out that Eq. (107) does not include the systematic uncertainty associated with the parameter χ_0 . While numbers hovering around $\chi_0 \sim 2 \text{ GeV}^{-2}$ seem to be favored by our analysis, the current spread of values for χ_0 from different theoretical estimations introduces a potential 10%-15% uncertainty in the hadronic light-by-light contribution. Therefore, we want to emphasize the need to put stronger bounds on the value of χ_0 . In particular, a lattice determination of χ_0 would be extremely useful.

Acknowledgments

We want to thank A. Nyffeler for correspondence and useful comments on the first version of this manuscript. O. C. wants to thank the University of Naples for very pleasant stays during the different stages of this work. L. C. and G. D'A. are supported in part by the EU under contract

MTRN-CT-2006-035482 (FLAVIANet), by MIUR, Italy, under project 2005-023102 and by Fondo dipartimentale per la ricerca 2009. O. C. is supported by the EU under contract MTRN-CT-2006-035482 (FLAVIANet) and by MICINN, Spain under grants FPA2007-60323 and Consolider-Ingenio 2010 CSD2007-00042 CPAN.

-
- [1] G. W. Bennett *et al.* [Muon g-2 Collaboration], Phys. Rev. Lett. **92**, 161802 (2004) [arXiv:hep-ex/0401008].
 - [2] J. Bijmans, E. Pallante and J. Prades, Nucl. Phys. B **626**, 410 (2002) [arXiv:hep-ph/0112255].
 - [3] M. Hayakawa and T. Kinoshita, Phys. Rev. D **57**, 465 (1998) [Erratum-ibid. D **66**, 019902 (2002)] [arXiv:hep-ph/9708227].
 - [4] M. Knecht and A. Nyffeler, Phys. Rev. D **65**, 073034 (2002) [arXiv:hep-ph/0111058].
 - [5] K. Melnikov and A. Vainshtein, Phys. Rev. D **70**, 113006 (2004) [arXiv:hep-ph/0312226].
 - [6] A. Nyffeler, Phys. Rev. D **79**, 073012 (2009) [arXiv:0901.1172 [hep-ph]].
 - [7] M. Knecht, A. Nyffeler, M. Perrottet and E. de Rafael, Phys. Rev. Lett. **88**, 071802 (2002) [arXiv:hep-ph/0111059].
 - [8] A. Nyffeler, arXiv:1001.3970 [Unknown].
 - [9] R. M. Carey *et al.*, FERMILAB-PROPOSAL-0989.
 - [10] J. Imazato, Nucl. Phys. Proc. Suppl. **129**, 81 (2004).
 - [11] D. Babusci *et al.*, arXiv:1007.5219 [Unknown].
 - [12] J. Prades, E. de Rafael and A. Vainshtein, arXiv:0901.0306 [hep-ph].
 - [13] F. Jegerlehner and A. Nyffeler, Phys. Rept. **477**, 1 (2009) [arXiv:0902.3360 [hep-ph]].
 - [14] J. M. Maldacena, Adv. Theor. Math. Phys. **2**, 231 (1998) [Int. J. Theor. Phys. **38**, 1113 (1999)].
 - [15] H. J. Behrend *et al.* [CELLO Collaboration], Z. Phys. C **49**, 401 (1991).
 - [16] F. Jegerlehner, Acta Phys. Polon. B **38**, 3021 (2007) [arXiv:hep-ph/0703125].
 - [17] A. E. Dorokhov and W. Broniowski, Phys. Rev. D **78**, 073011 (2008) [arXiv:0805.0760 [hep-ph]].
 - [18] G. D'Ambrosio, G. Isidori and J. Portoles, Phys. Lett. B **423**, 385 (1998) [arXiv:hep-ph/9708326].
 - [19] I. R. Klebanov and E. Witten, Nucl. Phys. B **556**, 89 (1999) [arXiv:hep-th/9905104].
 - [20] J. Erlich, E. Katz, D. T. Son and M. A. Stephanov, Phys. Rev. Lett. **95**, 261602 (2005).
 - [21] L. Da Rold and A. Pomarol, Nucl. Phys. B **721**, 79 (2005);
 - [22] T. Sakai and S. Sugimoto, Prog. Theor. Phys. **113**, 843 (2005);
 - [23] T. Sakai and S. Sugimoto, Prog. Theor. Phys. **114**, 1083 (2006)
 - [24] J. Hirn and V. Sanz, JHEP **0512**, 030 (2005);
 - [25] A. Karch, E. Katz, D. T. Son and M. A. Stephanov, Phys. Rev. D **74**, 015005 (2006)
 - [26] S. S. Gubser, I. R. Klebanov and A. M. Polyakov, Phys. Lett. B **428**, 105 (1998);
 - [27] E. Witten, Adv. Theor. Math. Phys. **2**, 253 (1998)
 - [28] C. T. Hill, Phys. Rev. D **73**, 126009 (2006).
 - [29] M. Gell-Mann, R. J. Oakes and B. Renner, Phys. Rev. **175**, 2195 (1968).
 - [30] E. Witten, Adv. Theor. Math. Phys. **2**, 505 (1998) [arXiv:hep-th/9803131].
 - [31] H. R. Grigoryan and A. V. Radyushkin, Phys. Rev. D **76**, 095007 (2007).
 - [32] H. R. Grigoryan and A. V. Radyushkin, Phys. Rev. D **77**, 115024 (2008) [arXiv:0803.1143 [hep-ph]].
 - [33] H. R. Grigoryan and A. V. Radyushkin, Phys. Rev. D **76**, 115007 (2007).
 - [34] H. R. Grigoryan and A. V. Radyushkin, Phys. Rev. D **78**, 115008 (2008) [arXiv:0808.1243 [hep-ph]].
 - [35] G. P. Lepage and S. J. Brodsky, Phys. Rev. D **22**, 2157 (1980).
 - [36] S. J. Brodsky and G. P. Lepage, Phys. Rev. D **24**, 1808 (1981).
 - [37] J. Gronberg *et al.* [CLEO Collaboration], Phys. Rev. D **57**, 33 (1998) [arXiv:hep-ex/9707031].
 - [38] B. Aubert *et al.* [The BABAR Collaboration], Phys. Rev. D **80**, 052002 (2009) [arXiv:0905.4778 [hep-ex]].
 - [39] M. F. L. Golterman and S. Peris, Phys. Rev. D **61**, 034018 (2000) [arXiv:hep-ph/9908252].
 - [40] M. Knecht and A. Nyffeler, Eur. Phys. J. C **21**, 659 (2001) [arXiv:hep-ph/0106034].
 - [41] C. Amsler *et al.* (Particle Data Group), Phys. Lett. B **667**, 1 (2008) and 2009 partial update for the 2010 edition.
 - [42] D. K. Hong and D. Kim, Phys. Lett. B **680**, 480 (2009) [arXiv:0904.4042 [hep-ph]].
 - [43] P. Ball, V. M. Braun and N. Kivel, Nucl. Phys. B **649**, 263 (2003) [arXiv:hep-ph/0207307].
 - [44] J. Rohrwild, JHEP **0709**, 073 (2007) [arXiv:0708.1405 [hep-ph]].
 - [45] A. Vainshtein, Phys. Lett. B **569**, 187 (2003) [arXiv:hep-ph/0212231].
 - [46] A. Gorsky and A. Krikun, Phys. Rev. D **79**, 086015 (2009) [arXiv:0902.1832 [hep-ph]].
 - [47] O. Cata, Phys. Rev. D **81**, 054011 (2010) [arXiv:0911.4736 [Unknown]].
 - [48] B. L. Ioffe and A. V. Smilga, Nucl. Phys. B **232**, 109 (1984).
 - [49] L. Cappiello, O. Cata and G. D'Ambrosio, arXiv:1004.2497 [Unknown].
 - [50] O. Cata and V. Mateu, JHEP **0709**, 078 (2007) [arXiv:0705.2948 [hep-ph]].